Brazilian Journal of Geophysics 40 (2022), 4, 511-521
Brazilian Geophysical Society
ISSN 2764-8044
DOI: 10.22564/brjg.v40i4.2191

EVALUATION OF THE DIX SCALING FACTOR DURING GEOMAGNETICALLY DISTURBED PERIODS OVER SOUTH AMERICA

Paulo França Barbosa-Neto [1,2*], Giorgio Arlan da Silva Picanço [1], Clezio Marcos De Nardin [3], Paulo Alexandre Bronzato Nogueira [4], Laysa Cristina Araújo Resende [1,5], Juliano Moro [6,7] and E. Romero-Hernandez [8]

[1]Instituto Nacional de Pesquisas Espaciais - INPE, Heliophysics Division, São José dos Campos, SP, Brazil
[2]Centro Universitário Christus - UNICHRISTUS, Engineering Department, Fortaleza, CE, Brazil
[3]Instituto Nacional de Pesquisas Espaciais - INPE, Directory, São José dos Campos, SP, Brazil
[4]Instituto Federal de Educação, Ciência e Tecnologia de São Paulo - IFSP, Jacareí, SP, Brazil
[5]National Space Science Center, Chinese Academy of Sciences, Beijing, China
[6]Laboratório Sino-Brasileiro para Clima Espacial - SKSW, Santa Maria, RS, Brazil
[7]Instituto Nacional de Pesquisas Espaciais - INPE, Southern Space Coordination, Santa Maria, RS, Brazil
[8]Universidad Autónoma de Nuevo León- UANL, Facultad de Ciencias Físico-Matemáticas, Monterrey, Mexico

*Corresponding author email: pafraneto@gmail.com

ABSTRACT. In this work, we present a study of the Total Electronic Content (TEC) spatiotemporal variability during geomagnetically disturbed periods over South America. For this, we evaluated the Disturbance Ionosphere indeX (DIX) scaling factor (ß coefficient) for different magnetic dip angles and seasons. In this context, the ß values are given in TEC units (TECU) and correspond to a latitudinal-dependent factor used to normalize the DIX output into a scale from 0 to 5. Thus, we selected thirteen magnetic storm events between 2013 and 2017, subdivided into seven moderate, four intense, and two extreme magnetic storms. The results showed that the ß coefficient latitudinal variation is characterized by two asymmetric crests concerning the magnetic equator. This suggests the presence of transequatorial thermospheric wind effects on the ionosphere's plasma distribution. Additionally, we observed that the crests occur close to the magnetic equator during the winter and autumn and at higher latitudes during summer and spring. Also, we noticed a drastic decrease in the daily highest ß-values before the Storm Sudden Commencement (SSC) stage of the studied events and during the magnetic storm recovery phase. This behavior highlights the expected scenario of quiet conditions with no TEC disturbance.

Keywords: ionosphere; Total Electron Content (TEC); Disturbance Ionosphere indeX (DIX); magnetic storms; GNSS

INTRODUCTION

In the last two decades, there has been a growing interest from the scientific community in developing new techniques for scaling the intensity of ionospheric effects triggered by different space weather phenomena, e.g., magnetic storms, Equatorial Plasma Bubbles (EPBs), and solar flares (Jakowski et al., 2006, 2012; Sanz et al., 2014; Denardini et al., 2020a; Picanço et al., 2020, 2022). Many of these efforts are motivated by the increasing expansion of the radio-based space systems, which are significantly susceptible to changes in the solar-terrestrial environment and may suffer severe damage during disturbed periods (Jakowski et al., 2012). In this context, recent studies focus mainly on assessing the capabilities of ionospheric scale indices regarding effects on the Global Navigation Satellite System (GNSS) networks during extreme space weather events, especially magnetic storms (Jakowski and Hoque, 2019; Borries et al., 2020; Denardini et al., 2020b; Picanço et al., 2021).

During magnetic storms, the Earth's ionosphere can undergo abrupt changes in the distribution and concentration of plasma. These changes can be monitored by analyzing the temporal variation of Total Electron Content (TEC) values. In this context, the TEC can be obtained from the analysis of propagation parameters of transionospheric GNSS signals and is commonly defined as a referential measure of the ionosphere plasma density as a function of free electrons (Picanço et al., 2022). In short, the TEC corresponds to the estimated number of free electrons in the ionized path along an imaginary tube with a cross-section of 1 m^2, whose ends are the satellite in orbit and a given ground receiver (Kersley et al., 2004).

Ionospheric storms are abrupt increases / decreases in the ionosphere plasma density, which generally occur due to changes in the thermosphere-ionosphere dynamics during disturbed periods (Matsushita, 1959). Specifically, the ionosphere's electron density can increase (decrease) during positive (negative) ionospheric storms. During negative storms, the main factor that promotes plasma reduction is the decrease in the O/N_2 ratio (Rishbeth, 1991; Fuller-Rowell et al., 1996). During positive storms, enhancements in the O/N_2 ratio, thermospheric winds, and disturbed electric fields are the main causes. In this regard, two types of disturbed electric fields can affect the ionosphere dynamics during magnetic storms: the Prompt Penetration Electric Field (PPEF) and the Disturbance Dynamo Electric Field (DDEF) (Nogueira et al., 2011; Moro et al., 2021). The PPEF is associated with changes in the Interplanetary Magnetic Field (IMF) polarity (Abdu, 1997). This phenomenon arises from the Interplanetary Electric Field (IEF) penetration into the Earth's high-latitudes ionosphere during its southward incursion. Then, the IEF is mapped to equatorial latitudes as an undershielding electric field (PPEF) with dawn-to-dusk polarity (Kikuchi et al., 2000). An overshielding penetration occurs when the IMF turns northwards after developing the shielding layer with dusk-to-dawn polarity. On the other hand, the DDEF is associated with the energy injection at high latitudes that causes auroral heating and results in a global change in the thermospheric circulation (Abdu, 1997; Prölls, 1997).

Following the demand for more ionospheric-monitoring tools, Jakowski et al. (2006) proposed the Disturbance Ionosphere indeX (DIX). In its first formulation, the DIX represented a proxy for the TEC-based response to magnetic storms. Later, the original DIX methodology evolved by incorporating new parameters and capabilities (Jakowski et al., 2012; Wilken et al., 2018; Jakowski and Hoque, 2019; Picanço, 2019; Denardini et al., 2020a; Picanço et al., 2020, 2021, 2022). The DIX currently corresponds to a scaled value of the ionospheric degree of perturbation during several space weather phenomena (e.g., magnetic storms, EPBs, and solar flares). Furthermore, the DIX values are assigned to an ionospheric scale that varies according to the intensity of the disturbances. In this context, Denardini et al. (2020a) proposed a scaling factor for their DIX version (named ß coefficient), which corresponds to a latitudinal dependent value used to normalize the DIX output into a scale that ranges from 0 to 5. The authors define the ß coefficient as a term for the latitudinal effects of magnetic storms (namely external drivers) on the ionosphere.

The primary purpose of this study is to evaluate the method proposed by Denardini et al. (2020a) to obtain the scaling factor for the DIX equation presented in their study. In this context, we performed a comparative analysis of the ß coefficient during different magnetic storm events over the South American region. We specifically focused on comprehending the seasonal and latitudinal disturbed TEC variability as a function of the magnetic dip angle for different latitude ranges over South America. For that, we selected a set of geomagnetically disturbed periods, including magnetic storm events, between 2013 and 2017. In order to evaluate the ß-related TEC spatiotemporal behavior during the selected periods, we divided the events into seven moderate, four intense, and two extreme storms. Our results show that significant characteristics of the regional ionosphere can be observed through the ß scaling factor, which could help highlight space weather effects over the South American region through the DIX usage.

METHODOLOGY

DIX calculation

We based this study on the DIX methodology presented in Denardini et al. (2020a) to analyze the disturbed TEC variations during selected magnetic storm periods over the South American ionospheric region. Therefore, we used the TEC maps provided by the "Brazilian Studies and Monitoring of Space Weather" (Embrace/INPE) (Takahashi et al., 2016), which derive from the procedure presented in Otsuka et al. (2002). The DIX is defined by equation 1:

$$\mathrm{DIX}_k(t) = \left| \frac{\alpha\left(\Delta TEC_k(t)/TEC_k^{Qd}(t)\right) + \Delta TEC_k(t)}{\beta} \right|, \quad (1)$$

From equation 1, the first term ($\Delta TEC_k = TEC_k(t) - TEC_k^{Qd}(t)$) represents the TEC percentual variation when comparing a given epoch ($TEC_k(t)$) to the non-perturbed reference ($TEC_k^{Qd}(t)$). More specifically, the $TEC_k^{Qd}(t)$ term corresponds to the non-perturbed reference calculated using the 3-hour moving average over the reference day and the term $TEC_k(t)$ is the TEC of the epoch of interest. This first part of the equation is multiplied by the α coefficient, which corresponds to the TEC_k^{Qd} values at local midnight. More details on the non-perturbed reference calculation can be found in Picanço et al. (2020). The ß coefficient is a latitudinal-dependent factor used to normalize the DIX output into a scale ranging from 0 to over 5. This value, given in TEC units (1 TECU = 10^{16}el/m^2), changes as a function of the magnetic storm latitudinal effects on the ionosphere. Therefore, this coefficient is essential in defining the DIX spatiotemporal resolution. The ß-coefficient calculation is defined in equation 2:

$$\beta_k(t) = \left| \frac{\alpha\left(\Delta TEC_k(t)/TEC_k^{Qd}(t)\right) + \Delta TEC_k(t)}{5} \right|, \quad (2)$$

Furthermore, the DIX provides a dimensionless disturbance level within a scale of ionospheric states. This scale ranges from 0 to over 5 (Table 1) according to the intensity of space weather phenomena detected using DIX, having as a level 5 reference the St. Patrick's Day magnetic storm (Denardini et al., 2020a):

Table 1: DIX scale of ionospheric states.

DIX	Ionospheric state
$0-1$	Quiet
$1-2$	Weakly Disturbed
$2-4$	Disturbed
$4-5$	Exceptionally Disturbed
>5	Extremely Disturbed

The β coefficient

The ß coefficient corresponds to the highest daily TEC value capable of normalizing the DIX on a scale from 0 to over 5 as a function of the magnetic dip angle. Thus, the ß-coefficient development considers South America's longitude and latitude extension.

Figure 1 shows the geographic locations of the TEC points (black dots) used in the ß-coefficient analysis over South America. The red line shows the magnetic equator (2015) coordinates taken from the International Geomagnetic Reference Field (IGRF), representing the 0° dip angle. The black lines represent the dip-angle variation on both magnetic hemispheres. We emphasize that the ß-points are inside a 5x5 degree cell, represented by the light gray squares. Additionally, the points cross each isoline with a 2.5-degree interval in longitude, resulting in 159 sampling locations. More details about the TEC maps used in this analysis can be seen in Takahashi et al. (2016).

Dataset and analysis

As mentioned before, we used TEC data provided by the EMBRACE/INPE database in this study. This way, the TEC values are calculated using data from about 200 GNSS receivers across the South American region. The final product available on the EMBRACE website is a set of TEC interpolated two-dimensional matrices (TEC maps) with a 0.5x0.5 degree spatial resolution every 10 minutes (Takahashi et al., 2016). In this regard, we emphasize that the ß-coefficient points are defined over these matrices to achieve a better spatial distribution of the sampling points.

It is essential to mention that developing DIX maps is not the main intent of this study. Instead, the primary purpose here is to evaluate the ß-coefficient reliability in representing the TEC spatiotemporal variability over South America, aiming to better comprehend the local ionospheric phenomena. In short, the main objective of this work is to understand how the magnitude of ionospheric disturbances varies with latitude during magnetic storm events of different intensities over South America.

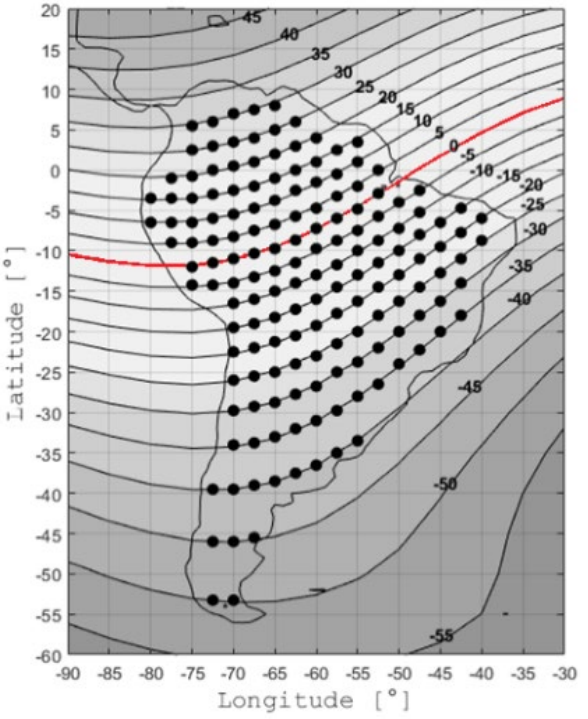

Figure 1: Geographic locations of the ß-coefficient points (black dots) over South America.

Therefore, we evaluated the ß-coefficient spatiotemporal variation during geomagnetically disturbed periods, considering the three days around each of the selected magnetic storms. For this selection, we analyzed the Disturbance storm time (Dst) index values before, during, and after each storm period. Furthermore, we analyzed a data set from 2013 to 2017. Then, we observed about 80 sudden impulses on the Dst index during these years, which were considered to identify the beginning of each geomagnetically disturbed period. Thus, we selected thirteen magnetic storm events classified into moderate ($-100\ nT \leq Dst \leq -50\ nT$; seven events), intense ($-200\ nT \leq Dst \leq -100\ nT$; four events), and extreme ($Dst \leq -200\ nT$; two events) (Gonzalez et al., 1994). The magnetic storm periods and some of their characteristics are shown in Table 2.

RESULTS

This section presents an analysis of the ß-coefficient spatiotemporal variation during periods with moderate, intense, and extreme magnetic storms. Therefore, we evaluated the ß-coefficient values according to the intensity of the selected magnetic storms at different periods along different magnetic dip/latitude ranges.

We organized our results according to the intensity of each selected magnetic storm. Figure 2

shows the ß-coefficient variation regarding the latitude/dip angle for seven selected moderate magnetic storms. Notice that the amplitude of the ß coefficient is given in TEC units, whose variation is evaluated in the range of 30 to -50 degrees in dip angle. Figure 3 shows the same type of data but for the four selected intense magnetic storms. This analysis is also reproduced in Figure 4, which sustains the evaluation of two extreme magnetic storm events. The black spots represent the values calculated using the ß-coefficient methodology. These points are the same 159 black spots distributed over the dip angle isolines ranging between 30 and -50 degrees, as previously described in Figure 1. In all cases, the red spots represent the average of the black spot values over the seven days previously considered in this analysis.

Figure 2 shows that the ß-coefficient behavior is characterized by two asymmetric crests concerning the magnetic equator. It is well known that a valley describes the daytime TEC latitudinal distribution at low latitudes at the magnetic dip equator flanked by two peaks, one on each side of the dip equator at about 15° in magnetic latitude. This behavior is known as the Equatorial Ionization Anomaly (EIA). Such two peaks with the latitudinal distribution of the ß coefficient are due to the presence of the EIA, highlighting the need for higher ß-values to achieve a believable DIX over tropical latitudes. Moreover, it is interesting to observe the asymmetry in the peaks during the summer and the spring. The highest ß amplitudes occurred mainly in the north region regarding the magnetic equator. Besides, during the winter and autumn, the highest amplitudes occurred mainly in the southern region.

Table 2: Moderate, intense, and extreme magnetic storm events used for the ß-coefficient analysis.

	Month, Year	Analyzed Period (Days)	SSC (Day, Hour)	Minimum of Main Phase (Day, Hour, Dst)
Moderate Storms	NOV-2013	06-07-08-09-10-11-12	08-21:00	09 – 09:00 -80 nT
	APR-2014	09-10-11-12-13-14-15	11-02:00	12-10:00 -87 nT
	AUG-2014	24-25-26-27-28-29-30	25-17:00	27-19:00 -79 nT
	SEP-2014	10-11-12-13-14-15-16	11-23:44	13-00:00 -88 nT
	DEC-2014	19-20-21-22-23-24-25	21-19:11	22-06:00 -71 nT
	JAN-2015	04-05-06-07-08-09-10	07-06:16	07-12:00 -99 nT
	MAY-2016	05-06-07-08-09-10-11	07-22:00	08-09:00 -88 nT
Intense Storms	FEB-2014	16-17-18-19-20-21-22	18-14:00	19-09:00 -119 nT
	DEC-2015	17-18-19-20-21-22-23	19:16:16	20-23:00 -155 nT
	JAN-2016	29-30-31-01-02-03-04	31-00:49	01-01:00 -110 nT
	SEP-2017	05-06-07-08-09-10-11	06-23:43	08-02:00 -124 nT
Extreme Storms	MAR-2015	14-15-16-17-18-19-20	17-04:45	17-23:00 -222 nT
	JUN-2015	20-21-22-23-24-25-26	22-18:30	23-05:00 -204 nT

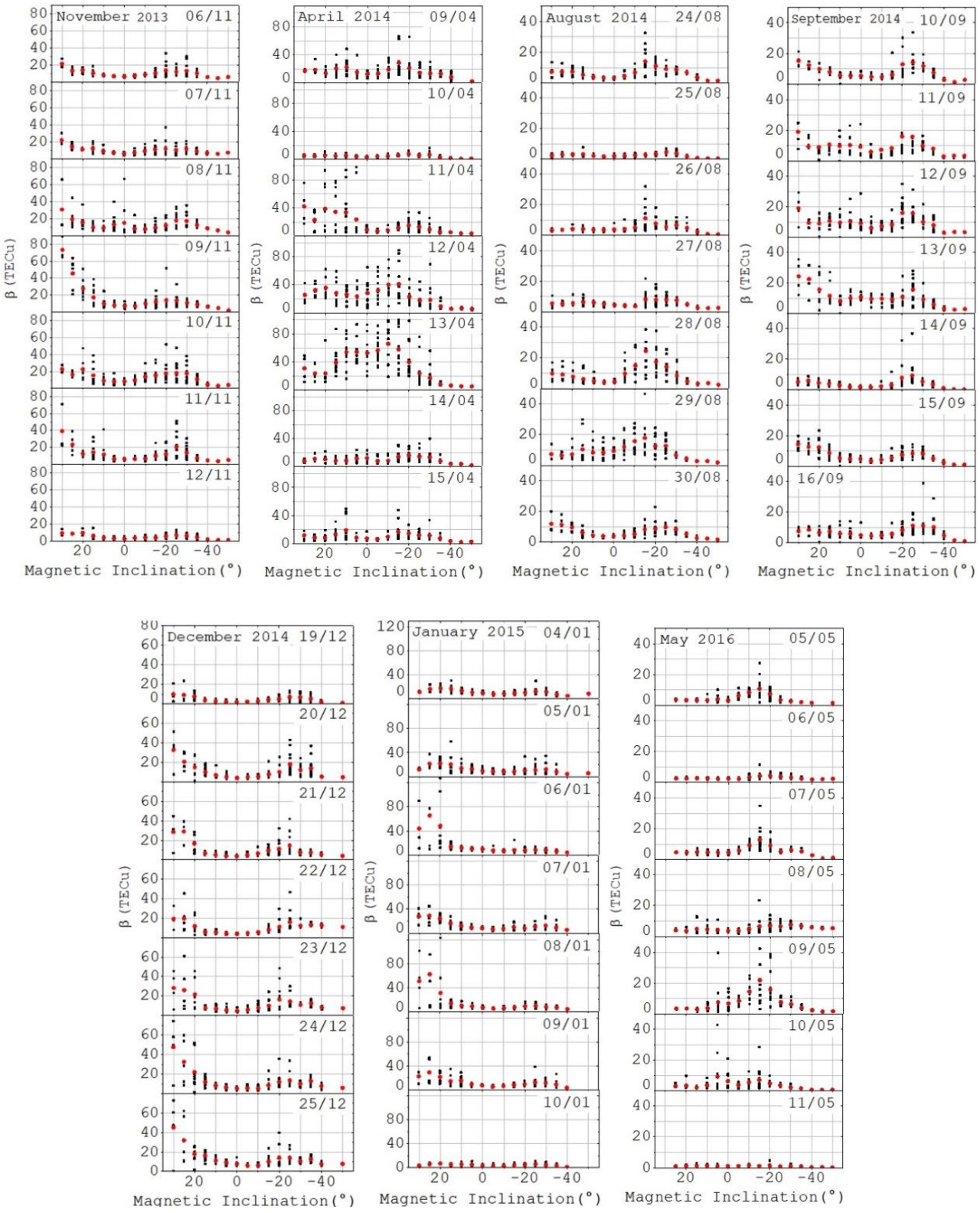

Figure 2: Latitudinal distribution of the ß-coefficient analysis during the moderate storm periods.

This asymmetry between the northern and southern crests concerning the magnetic equator indicates the transequatorial thermospheric wind effects on the TEC. These winds interact with the ionized particles through the ion drag, changing the ratio of atomic oxygen number density to molecular nitrogen number density ([O]/[N2]) and, consequently, the ionospheric behavior (Richmond et al., 1992). In all ß coefficient latitudinal distribution figures, it is possible to notice that the transequatorial winds are blowing northward (southward) during the summer (winter), dragging the ionization to the northern (southern) crest and accumulating the ionospheric content in the regions concerning the magnetic

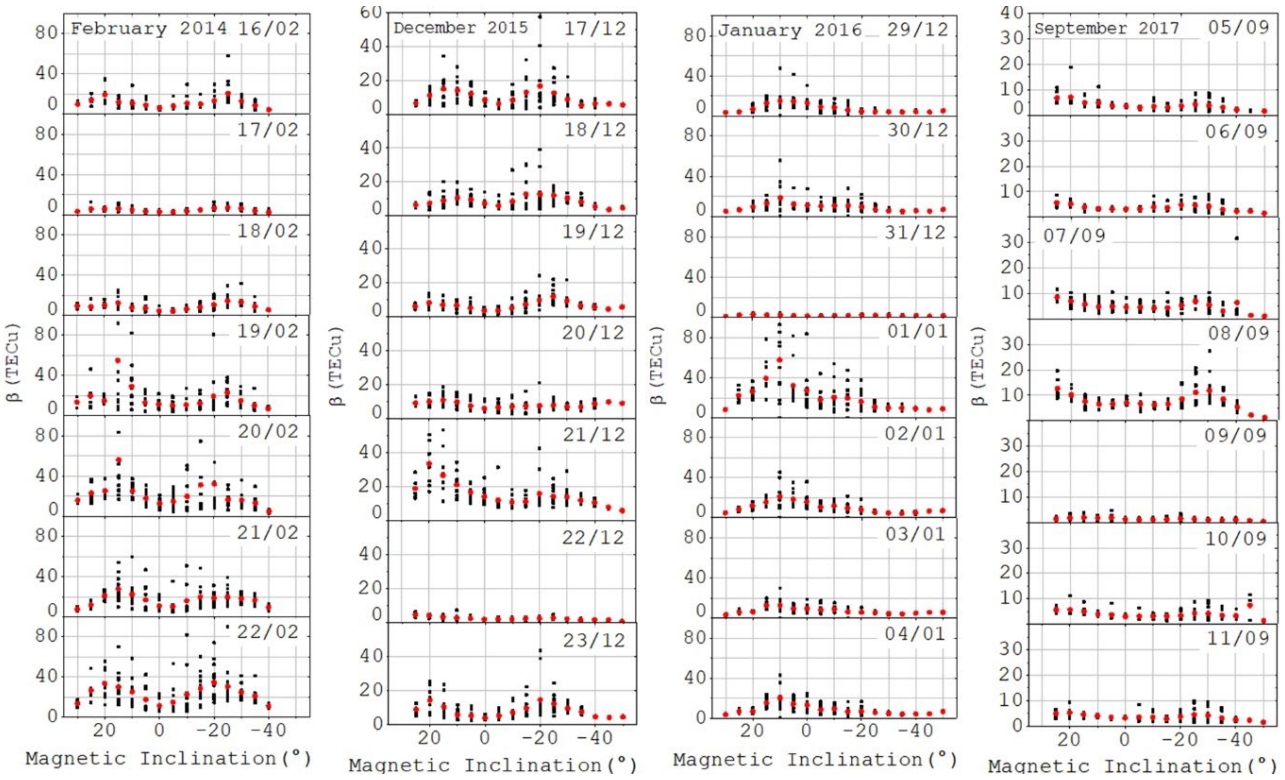

Figure 3: Latitudinal distribution of the ß-coefficient analysis during the intense storm periods.

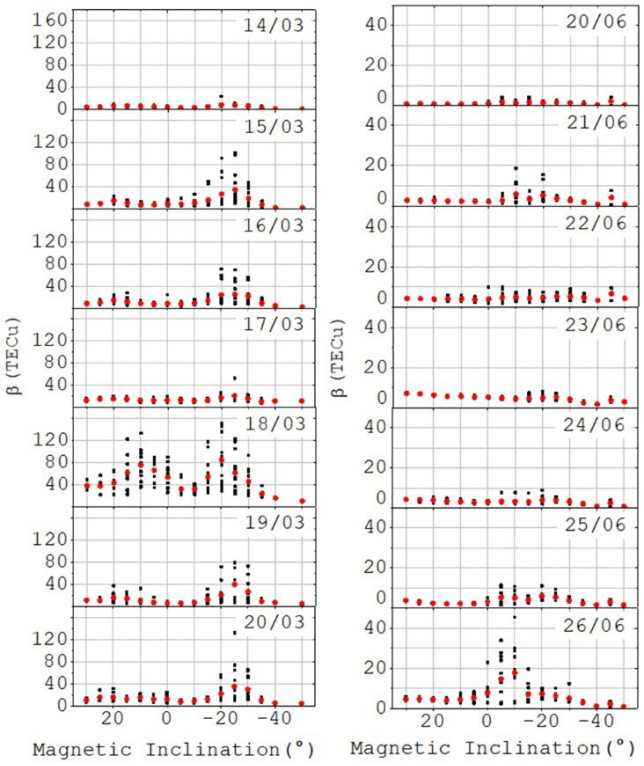

Figure 4: Latitudinal distribution of the ß-coefficient analysis during the extreme storm periods.

equator. In this scenario, because of these ionized particles' movement in the summer hemisphere, a decrease of the [O]/[N2] ratio changes the ion production/loss term with a reduction in the [O] concentration and an enhancement in the N2 concentration. In the winter hemisphere, the opposite effect can be seen with an increase in the [O]/[N2] ratio caused by the ion exchange process, where there is a reduction in the N2 concentration. As it is well known, these chemistry variations directly affect the electron content since O^+ is the major ionosphere ionic constituent of the F2 region (England et al., 2010).

In addition to this asymmetry, the crests occurred close or away from the magnetic equator, depending on the season. The results showed in fig2Figure 2 suggest that this occurrence is associated with convergent and divergent meridional winds. The highest ß values occurred close to the magnetic equator during the winter (August 2014) and the autumn (April 2014 and May 2016), influenced by the action of the convergent wind. In a convergent meridional wind, the ionospheric plasma is moved equatorward, increasing the electron content in the regions close to the magnetic equator (Rishbeth, 1991). During the summer (December 2014 and January 2015) and the spring (November 2013 and September 2014), the highest ß values occurred away from the magnetic equator due to the divergent meridional winds' action. In the presence of a divergent meridional wind (poleward), the ionized particles are dragged to the regions away from the magnetic equator and moved to the lower altitudes where the recombination loss rate is more significant than the production rate. As a result of the ion-drag effect and the recombination loss process, there is a decrease in the TEC, and the crests develop in the regions away from the magnetic equator (Fagundes, 1995; Titheridge, 1995; Batista, 2011). Our analyses here agreed with the results of Mendillo et al. (2000), in which they confirm that the meridional wind action also enhances the electron content in one of the EIA crests (e.g., November 2013 and January 2015).

Figure 3 and Figure 4 show the ß coefficient values estimated during the intense and extreme magnetic storms, respectively. These figures follow the exact description of the first sequence previously presented in Figure 2. The results confirm the seasonal behavior of the highest daily ß values. However, we noticed that there is one more interesting feature of the ß coefficient behavior: a drastic decrease of the daily highest ß values mainly in the period before the SSC (17/02 – Figure 3; 14/03 and 20/06 – Figure 4) and during the magnetic storm recovery phase (on 22/12 and 09/09 – Figure 3). We observed that the ß coefficient values decreased during the magnetic storm main phase only in the case of 31/12, and the low ß values prior to SSC highlight the quiet condition with no TEC disturbance.

On the other hand, during the storm's main phase, it should indicate a negative ionospheric storm, which indicates the DDEF action. During the magnetic storms, the auroral heating originates the disturbed thermospheric winds producing a daytime westward electric field that intensifies the action of the downward vertical $\boldsymbol{E} \times \boldsymbol{B}/B^2$ plasma drift over the equator (Sreeja et al., 2009; Batista et al., 2011). The vertical drift moves the plasma to low altitudes where the loss processes are more effective than the production processes and cause an EIA inhibition due to plasma fountain suppression.

Returning to the asymmetry of the crests, we mentioned before that it is indicative of the transequatorial thermospheric wind effects on the ionosphere electron content, which interact with the ionized particles through the ion-drag, changing the ratio of atomic oxygen number density to molecular nitrogen number density ([O]/[N2]), and consequently the ionosphere behavior. Moreover, the crests occurred close to the magnetic equator during the winter and the autumn, influenced by the action of the convergent wind (equatorward), and occurred way from the magnetic equator during summer and the spring as a result of the divergent meridional winds' action (poleward). The interpolated maps of the thermospheric [O]/[N2] ratio obtained by the Global Ultraviolet Imager (GUVI) satellite (Christensen et al., 2003) between January 04 and 10, 2015, are presented in Figure 5. The blank region represents the South America Magnetic Anomaly (SAMA) location, which is out of the scope of our study. The maps' sequence follows the same idea presented in Figure 2: 7 days considering three days before the Dst minimum value (05/01 and 06/01), the minimum Dst day (07/01), and the three consecutive days (08/01, 09/01 and 10/01). On 04/01, 05/01 and 07/11, the [O]/[N2] ratio values for the magnetic equator are similar for the northern and southern regions. However, on the other days, especially on 10/11, an ion drag changed the atomic oxygen number density ratio to molecular nitrogen number density. Thus, the transequatorial winds blow northward, dragging the ionization from the southern hemisphere to the northern hemisphere. Therefore, this behavior agrees with the ß-coefficient values derived for the same period.

Additionally, based on the variability of the ß values showed in Figures 2, 3 and 4, we present in Figure 6 the latitudinal (y-axes) and seasonal (x-axes) dependence of ß values (color bar) based on data obtained from all the selected magnetic storms. The color bar is supposed to estimate the largest TEC disturbances based on the averaged ß values plus one positive standard deviation of the highest daily ß values. This one positive standard deviation allowed us to build the seasonal profile of an extreme event as a function of dip latitude during the disturbed periods based on the ß coefficient. The solid red line represents this extreme profile in Figure 6. On the left side of Figure 6 we show the disturbance level within the color scale from non-disturbed (blue) to extremely disturbed (red) in TECU. We observed the most significant disturbances occurring over March under the extreme magnetic storm (17/03, St Patrick's magnetic storm), causing a drastic perturbation over the south crest of the equatorial ionization anomaly. All over the studied months, the most significant disturbances occurred over the EIA crest, which shows that the perturbations over the plasma transport (electric field and thermospheric winds) were more significant than the production and loss terms.

The right-side panel in Figure 6 shows the estimated extreme ß profile drastically influenced by the magnetic storms that occurred in the summer and

the autumn. Its effects are greater at 20°S and 30°S than in other regions concerning the magnetic equator. During the winter and the spring, the disturbing effects of the magnetic storms are more significant at 10°N and 30°N. The behavior of the ß coefficient shows that the different magnetic storms affect the ionosphere differently, and there is a tendency that its response is more dependent on the seasonality than on the magnetic storm intensity. This difference in the intensity of the ionosphere responses during disturbed periods can be explained by the semiannual variation in TEC, where the global mean TEC values are larger for equinoxes than for solstices (Kelley, 2009). Therefore, the extreme ß profile as a function of the dip latitude and the season must be used to estimate the DIX maps 2013 and 2017.

Finally, our results indicate a strict relationship between the amplitude of the ß coefficient and seasonality in South America. Therefore, these factors must be considered in the calculation of the DIX so that this index have better reliability.

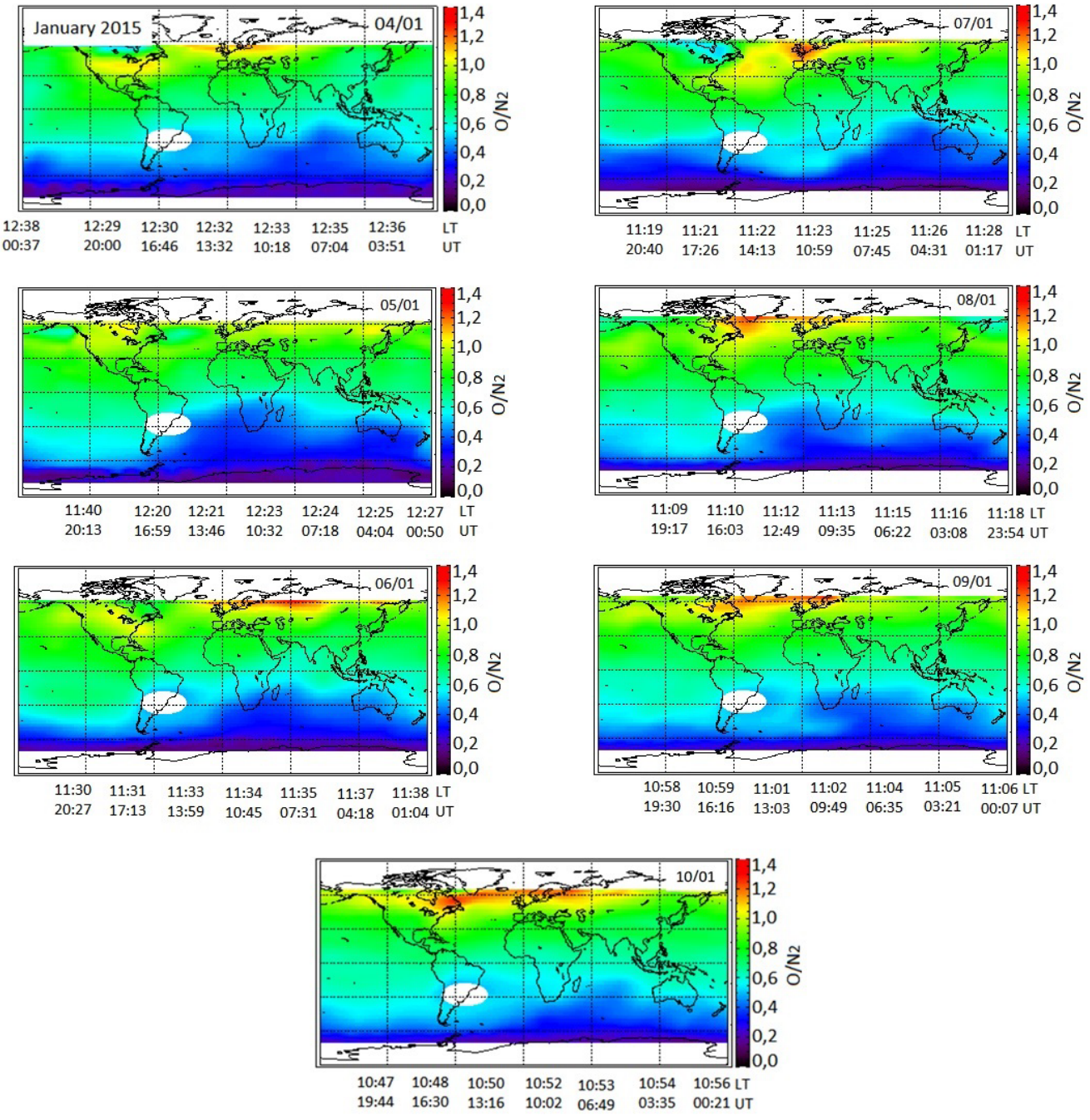

Figure 5: Global maps of the thermospheric [O]/[N2] ratio obtained by the GUVI satellite between January 04 and 10, 2015.

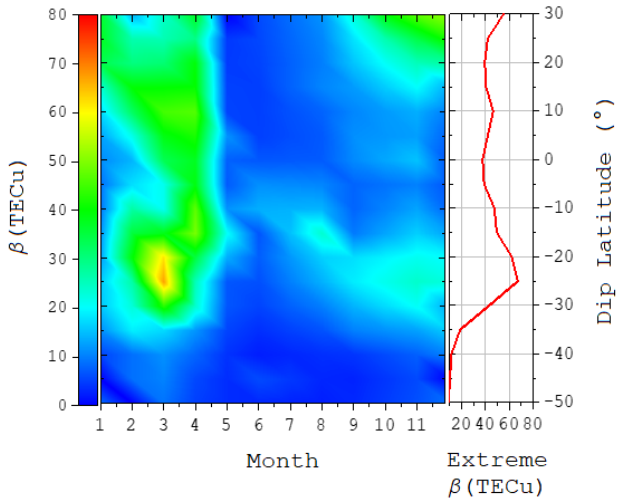

Figure 6: Coefficient ß spatiotemporal variation during the selected geomagnetically disturbed periods.

CONCLUSIONS

This study presented an analysis of the influence of magnetic latitude and seasonal variability on calculating the DIX spatiotemporal scaling factor over South America during thirteen magnetic storms (seven moderate, four intense, and two extreme magnetic storms in the 2013-2017 period). Furthermore, based on the latitudinal evolution of the ß coefficient, we identified a close relation with the TEC latitudinal and seasonal variability, proving its capability to normalize the DIX on a scale between 0 and 5.

The results showed that the ß-coefficient spatiotemporal variation was characterized by two asymmetric crests concerning the magnetic equator. The ß coefficient crests occurred due to the presence of the EIA. It is well known that the daytime TEC latitudinal distribution at low latitudes is characterized by two peaks, one on each side of the dip equator at about 15° magnetic latitude. The asymmetry between the crests is indicative of the transequatorial thermospheric wind effects on the ionosphere electron content, which interact with the ionized particles through the ion-drag, changing the ratio of atomic oxygen number density to molecular nitrogen number density ([O]/[N2]) and consequently the ionosphere behavior. Moreover, the crests occurred close to the magnetic equator during the winter and the autumn, influenced by the action of the convergent wind (equatorward) and occurred way from the magnetic equator during summer and the spring of the divergent meridional winds' action (poleward).

We noticed a drastic decrease in the daily highest ß values, mainly in the period before the SSC and during the magnetic storm recovery phase. The low ß values prior to SSC highlight the quiet condition with no TEC disturbance. However, the storm main phase should indicate a negative ionospheric storm. The lack of the ß highest daily values during the recovery phase indicates the DDEF action. During the magnetic storms, the auroral heating originates the disturbed thermospheric winds producing a daytime westward electric field that intensifies the action of the downward vertical ExB/B^2 plasma drifts over the equator. The vertical drift moves the plasma to low altitudes where the loss processes are more effective than the production processes and cause an EIA inhibition due to plasma fountain suppression.

Based on the variability of the ß values estimated for the 13 magnetic storms, we built the seasonal profile of an extreme event as a function of dip latitude during the disturbed periods based on the ß coefficient. This profile showed that the largest disturbances occurred over March 2015, under the effect of St Patrick's extreme magnetic storm. It resulted in a drastic perturbation over the south crest of the EIA. Moreover, we also noticed that over the months, the most significant disturbances occur over the EIA crest, which shows that the perturbations over the plasma transport (electric field and thermospheric winds) were more significant than the production and loss terms.

Data and Materials Availability

The data used in the present study are fully open source and accessible on the Embrace/INPE Program website (http://www.inpe.br/spaceweather). The thermospheric [O]/[N2] data can be obtained from the GUVI (Global Ultraviolet Imager) website (http://guvitimed.jhuapl.edu).

REFERENCES

Abdu, M. A.,1997, Major phenomena of the equatorial ionosphere-thermosphere system under disturbed conditions: Journal of Atmospheric and Solar-Terrestrial Physics, **59**, 13, 1505–1519. doi: 10.1016/s1364-6826(96)00152-6.

Batista, I. S., Diogo, E. M., Souza, J. R., Abdu, M. A., and Bailey, G. J, 2011, Equatorial Ionization Anomaly: The Role of Thermospheric Winds and the Effects of the Geomagnetic Field Secular Variation, *in*: Abdu, M., Pancheva, D., eds., Aeronomy of the Earth's Atmosphere and Ionosphere. IAGA Special Sopron Book Series, **2**. Springer, Dordrecht, 317–328. doi: 10.1007/978-94-007-0326-1_23.

Borries, C., Wilken, V., Jacobsen, K. S., García-Rigo, A., Dziak-Jankowska, B., Kervalishvili, G., Jakowski, N., Tsagouri, I., Hernández-Pajares, M., Ferreira, A. A., and Hoque, M. M., 2020, Assessment of the capabilities and applicability of ionospheric perturbation indices provided in Europe: Adv. Space Res., **66**, 546–562. doi: 10.1016/j.asr.2020.04.013.

Christensen, A. B., 2003, Initial observations with the Global Ultraviolet Imager (GUVI) in the NASA TIMED satellite mission: Journal of Geophysical Research, **108**, A12. doi: 10.1029/2003ja009918.

Denardini, C. M., Picanço, G. A. S., Barbosa Neto, P. F., Nogueira, P. A. B., Carmo, C. S., Resende, L. C. A., Moro, J., Chen, S. S., Romero-Hernandez, E., Silva, R. P., and Bilibio, A. V., 2020a, Ionospheric Scale Index Map Based on TEC Data for Space Weather Studies and Applications: Space Weather, **18**, 9. doi: 10.1029/2019sw002328.

Denardini, C. M., Picanço, G. A. S., Barbosa Neto, P. F., Nogueira, P. A. B., Carmo, C. S., Resende, L. C. A., Moro, J., Chen, S. S., Romero-Hernandez, E., Silva, R. P., and Bilibio, A. V., 2020b, Ionospheric Scale Index Map Based on TEC Data during the Saint Patrick Magnetic Storm and EPBs: Space Weather, **18**, 9. doi: 10.1029/2019sw002330.

England, S. L., Immel, T. J., Huba, J. D., Hagan, M. E., Maute, A., and Demajistre, R., 2010, Modeling of multiple effects of atmospheric tides on the ionosphere: An examination of possible coupling mechanisms responsible for the longitudinal structure of the equatorial ionosphere: Journal of Geophysical Research: Space Physics, **115**, A5, A05308. doi: 10.1029/2009ja014894.

Fagundes, P. R, Sahai, Y., Bittencourt, J. A., and Takahashi, H., 1995, Observations of thermospheric neutral winds and temperatures at Cachoeira Paulista (23°S, 45°W) during a geomagnetic storm: Advances in Space Research, **16**, 5, 27–30. doi: 10.1016/0273-1177(95)00169-F.

Fuller-Rowell, T. J., Codrescu, M. V., Rishbeth, H., Moffett, R. J., and Quegan, S., 1996, On the seasonal response of the thermosphere and ionosphere to geomagnetic storms: J. Geophys. Res.-Space, **101**, 2343–2353. doi: 10.1029/95ja01614.

Gonzalez, W. D., Joselyn, J. A., Kamide, Y., Kroehl, H. W., Rostoker, G., Tsurutani, B. T., and Vasyliunas, V. M., 1994, What is a geomagnetic storm?: Journal of Geophysical Research, **99**, A4, 5771. doi: 10.1029/93ja02867.

Jakowski, N., Stankov, S. M., Schlueter, S., and Klaehn, D., 2006, On developing a new ionospheric perturbation index for space weather operations: Advances in Space Research, **38**, 11, 2596–2600. doi: 10.1016/j.asr.2005.07.043.

Jakowski, N., Borries, C., and Wilken, V., 2012, Introducing a disturbance ionosphere index: Radio Science, **47**, 4. doi: 10.1029/2011rs004939.

Jakowski, N. and Hoque, M. M., 2019, Estimation of spatial gradients and temporal variations of the total electron content using ground based GNSS measurements: Space Weather, **17**, 339–356. doi: 10.1029/2018sw002119.

Kelley, M. C., 2009, The Earth's ionosphere: Plasma physics and electrodynamics, 2nd ed., London WC1X 8RR, UK: Elsevier, Academic Press.

Kersley, L., Malan, D., Pryse, S. E., Cander, L. R., Bamford, R. A., Belehaki, A., Leitinger, R., Radicella, S. M., Mitchell, C. N., and Spencer, P. S. J., 2004, Total electron content: a key parameter in propagation: measurement and use in ionospheric imaging: Ann. Geophys., **47**, 1067–1091, 10.4401/ag-3286.

Kikuchi, T., Lühr, H., Schlegel, K., Tachihara, H., Shinohara, M., and Kitamura, T.-I., 2000, Penetration of auroral electric fields to the equator during a substorm: Journal of Geophysical Research: Space Physics, **105**, A10, 23251–23261. doi: 10.1029/2000ja900016.

Matsushita, S., 1959, A study of the morphology of ionospheric storms: Journal of Geophysical Research, **64**, 3, 305–321. doi: 10.1029/jz064i003p00305.

Mendillo, M., Lin, B., and Aarons, J., 2000, The application of GPS observations to equatorial aeronomy: Radio Science, **35**, 3, 885–904. doi: 10.1029/1999rs002208.

Moro, J., Xu, J., Denardini, C. M., Resende, L. C. A., Barbosa Neto, P. F. B., Da Silva, L. A., Silva, R. P., Chen, S. S., Picanço, G. A. S., Carmo, C. S., Liu, Z., Yan, C., Wang, C., and Schuch, N. J., 2021, First look at a geomagnetic storm with Santa Maria Digisonde data: *F* region responses and comparisons over the American sector. Journal of Geophysical Research: Space Physics, **126**, e2020JA028663. doi: 10.1029/2020ja028663.

Nogueira, P. A. B., Abdu, M. A., Batista, I. S., and De Siqueira, P. M., 2011, Equatorial ionization anomaly and thermospheric meridional winds during two major storms over Brazilian low latitudes. Journal of Atmospheric and Solar-Terrestrial Physics, **73**, 11-12, 1535–1543. doi: 10.1016/j.jastp.2011.02.008.

Otsuka, Y., Ogawa, T., Saito, A., Tsugawa, T., Fukao, S., and Miyazaki, S., 2002, A new technique for mapping of total electron content using GPS network in Japan: Earth, Planets and Space, **54**, 1, 63–70. doi: 10.1186/bf03352422.

Picanço, G. A. S., 2019, Desenvolvimento e análise de um índice ionosférico baseado em dados de Conteúdo Eletrônico Total. 2019. 190 p. Master's Degree in Space Geophysics, Instituto Nacional de Pesquisas Espaciais (INPE), São José dos Campos, SP, Brazil.

Picanço, G. A. S., Denardini, C. M., Nogueira, P. A. B., Barbosa-Neto, P. F., Resende, L. C. A., Carmo, C. S., Romero-Hernandez, E., Chen, S. S., Moro, J., and Silva, R. P., 2020, Evaluation of the non-perturbed TEC reference of a new version of the DIX: Braz. J. Geophys., **38**, 1–10. doi: 10.22564/rbgf.v38i3.2056.

Picanço, G. A. S., Denardini, C. M., Nogueira, P. A. B., Barbosa-Neto, P. F., Resende, L. C. A., Chen, S. S., Carmo, C. S., Romero-Hernandez, E., and Silva, R. P., 2021, Equatorial ionospheric response to storm-time electric fields during two intense

geomagnetic storms over the Brazilian region using a Disturbance Ionosphere index: Journal of Atmospheric and Solar-Terrestrial Physics, **223**, 105734. doi: 10.1016/j.jastp.2021.105734.

Picanço, G. A. S., Denardini, C. M., Nogueira, P. A. B., Resende, L. C. A., Carmo, C. S., Chen, S. S., Barbosa-Neto, P. F., and Romero-Hernandez, E. 2022, Study of the equatorial and low-latitude total electron content response to plasma bubbles during solar cycle 24–25 over the Brazilian region using a Disturbance Ionosphere index: Ann. Geophys., **40**, 503–517. doi: 10.5194/angeo-40-503-2022.

Prölss, G. W., 1997, Magnetic storm associated perturbations of the upper atmosphere: Geophysical Monograph Series, 227–241. doi: 10.1029/gm098p0227.

Richmond, A. D., Ridley, E. C., and Roble, R. G., 1992, A thermosphere/ionosphere general circulation model with coupled electrodynamics: Geophysical Research Letters, **19**, 6, 601–604. doi: 10.1029/92gl00401.

Rishbeth, H., 1991, *F*-Region Storms and Thermospheric Dynamics. Journal of Geomagnetism and Geoelectricity, **43**, 513–524. doi: 10.5636/jgg.43.Supplement1_513.

Sanz, J., Juan, J. M., González-Casado, G., Prieto-Cerdeira, R., Schlüter, S., and Orús, R., 2014, Novel Ionospheric Activity Indicator Specifically Tailored for GNSS Users, Proceedings of the 27th International Technical Meeting of the Satellite Division of The Institute of Navigation (ION GNSSC2014), Tampa, Florida, USA, 1173–1182, Institute of Navigation (ION), www.ion.org/publications/abstract.cfm?articleID=12269 (Access: 18 July 2022).

Sreeja, V., Ravindran, S., Pant, T. K., Devasia, C. V., and Paxton, L. J., 2009, Equatorial and low-latitude ionosphere-thermosphere system response to the space weather event of August 2005. Journal of Geophysical Research: Space Physics, **114**(A12), A12307. doi: 10.1029/2009ja014491.

Takahashi, H., Wrasse, C., Denardini, C. M., Pádua, M., De Paula, E., Costa, S., Otsuka, Y., Shiokawa, K., Monico, J., Ivo, A., and Sant'anna, N., 2016, Ionospheric TEC Weather Map Over South America. Space Weather, **14(11)**, 937–949. doi: 10.1002/2016sw001474.

Titheridge, J. E., 1995, Winds in the ionosphere — A review. Journal of Atmospheric and Terrestrial Physics, **57**, 14, 1681–1714. doi: 10.1016/0021-9169(95)00091-F.

Wilken, V., Kriegel, M., Jakowski, N., and Berdermann, J., 2018, An ionospheric index suitable for estimating the degree of ionospheric perturbations: Journal of Space Weather and Space Climate, **8**, A19. doi: 10.1051/swsc/2018008.

Barbosa-Neto, P.F.: conceptualization, data analysis, writing - original draft; **Picanço, G.A.S.:** GNSS data processing, code development for DIX calculation, data analysis; **De Nardin, C.M.:** interplanetary data analysis processing, study result discussion; **Nogueira, PA.B.:** interplanetary data analysis processing, study result discussion; **Resende, L.C.A.:** study design, data analysis; **Moro, J.:** study design, data analysis; **E. Romero-Hernandez:** study design, data analysis;

Received on October 17, 2022 / Accepted on April 20, 2023